

Water depth dependence of long-range correlation in nontidal variations in seafloor pressure

Tomohiro Inoue¹, Yoshihiro Ito², Laura Wallace³, Yutaka Yoshikawa⁴, Daisuke Inazu⁵, Emmanuel Soliman Garcia⁶, Tomoya Muramoto⁷, Kazuaki Ohta⁸, Syuichi Suzuki⁹, Ryota Hino⁹, and Spahr C Webb¹⁰

¹Graduate School of Science, Kyoto University

²Disaster Prevention Research Institute, Kyoto University

³GNS Science

⁴Kyoto University

⁵Tokyo University of Marine Science and Technology

⁶Disaster Prevention Research Institute, Kyoto university

⁷National Institute of Advanced Industrial Science and Technology (AIST)

⁸National Research Institute for Earth Science and Disaster Resilience, Tsukuba, Japan

⁹Tohoku University

¹⁰Lamont Doherty Earth Observatory

November 26, 2022

Abstract

Isolating the source of non-tidal oceanographic noise in seafloor pressure data is critical for improving the use of these data for seafloor geodetic applications. Residuals between nearby bottom pressure records have typically been used to remove the non-tidal components, as these are largely common-mode. To evaluate the similarities between pairs of observed bottom pressure records at a range of water depths, we calculate the standard deviations of the time series of residuals between data from all site pairs, recorded during a recent experiment offshore New Zealand. Similar to a recent study offshore Cascadia, we find that the magnitude of the standard deviation depends more on relative water depth than the distance between sites. This confirms that non-tidal components are more similar along isobaths even if the distance between sites is large. We show that the depth range varies with the depth of the deeper site of the pairs under restrictions.

Hosted file

supplement_v200812_sub.docx available at <https://aurelia.com/users/556372/articles/606416-water-depth-dependence-of-long-range-correlation-in-nontidal-variations-in-seafloor-pressure>

1
2 **Water depth dependence of long-range correlation in nontidal variations in seafloor**
3 **pressure**
4

5 **Tomohiro Inoue¹, Yoshihiro Ito², Laura M. Wallace^{3,4}, Yutaka Yoshikawa¹, Daisuke Inazu⁵,**
6 **Emmanuel Soliman Mortel Garcia², Tomoya Muramoto⁶, Kazuaki Ohta⁷, Syuichi Suzuki⁸,**
7 **Ryota Hino⁸, Spahr C. Webb⁹**

8
9 ¹ Graduate School of Science, Kyoto University, Kyoto, Japan

10 ² Disaster Prevention Research Institute, Kyoto University, Uji, Japan

11 ³GNS Science, Lower Hutt, New Zealand

12 ⁴Institute for Geophysics, University of Texas at Austin, Austin, TX, USA

13 ⁵Department of Marine Resource and Energy, Tokyo University of Marine Science and
14 Technology, Tokyo, Japan

15 ⁶National Metrology Institute of Japan, National Institute of Advanced Industrial Science and
16 Technology, Tsukuba, Japan

17 ⁷National Research Institute for Earth Science and Disaster Resilience, Tsukuba, Japan

18 ⁸Graduate School of Science, Tohoku University, Sendai, Japan

19 ⁹Lamont-Doherty Earth Observatory, Columbia University, Palisades, NY, USA
20

21 Corresponding author: Tomohiro Inoue (inoue.tomohiro.48n@st.kyoto-u.ac.jp)
22

23 **Key Points:**

- 24 • The similarity of the non-tidal components of bottom pressure varies with relative water
25 depth, rather than distance between sites.
- 26 • Bottom pressure data show that reference sites at similar depths will optimize
27 oceanographic noise removal for seafloor geodetic studies.
- 28 • Oceanographic models with baroclinicity reproduce the depth dependence of the nontidal
29 variations better than barotropic models.
30

31 **Abstract**

32 Isolating the source of non-tidal oceanographic noise in seafloor pressure data is critical for
33 improving the use of these data for seafloor geodetic applications. Residuals between nearby
34 bottom pressure records have typically been used to remove the non-tidal components, as these
35 are largely common-mode. To evaluate the similarities between pairs of observed bottom
36 pressure records at a range of water depths, we calculate the standard deviations of the time
37 series of residuals between data from all site pairs, recorded during a recent experiment offshore
38 New Zealand. Similar to a recent study offshore Cascadia, we find that the magnitude of the
39 standard deviation depends more on relative water depth than the distance between sites. This
40 confirms that non-tidal components are more similar along isobaths even if the distance between
41 sites is large. We show that the depth range varies with the depth of the deeper site of the pairs
42 under restrictions.

43 **Plain Language Summary**

44 Coherent signals of ocean bottom pressure are observed along common water depths
45 within an ocean bottom pressure array offshore New Zealand. We statistically evaluated the
46 similarity of the seafloor pressure collected in 2014 offshore the North Island's east coast, where
47 the Pacific Plate dives or "subducts" along the Hikurangi subduction zone beneath the North
48 Island. This is important for removal of noise caused by oceanographic processes, which must be
49 done to detect centimeter-level vertical movement of the seafloor crust during slow slip events
50 using seafloor pressure records. We measured the similarity of pairs of seafloor pressure records
51 at a range of water depths. Similar to a recent study offshore the Cascadia subduction zone, our
52 results confirm that seafloor pressure records from similar depths (but at large horizontal
53 distances from each other) can be used effectively to reduce oceanographic noise in sea floor
54 pressure data to reveal the seafloor crustal deformation.

55

56 **1. Introduction**

57 Temporal fluctuations in ocean bottom pressure originate from phenomena at varying
58 spatio-temporal scales over the Earth's surface driven by atmospheric and oceanic circulation,
59 tides, tsunamis, and tectonic deformation of the crust. Ocean-bottom pressure gauges (OBPs) are
60 becoming widely used to measure tectonic signals, particularly those caused by tectonic
61 deformation in some subduction zones (e.g., Menemenlis et al., 2008 (ECCO2); Inazu et al.,
62 2012 (IN12); Ito et al., 2011, 2013; Hino et al., 2014; Davis et al., 2015; Suzuki et al., 2016;
63 Wallace et al., 2016; Sato et al., 2017; Muramoto et al., 2019; Fredrickson et al., 2019). Previous
64 studies have used OBPs to record vertical seafloor deformation during episodic slow slip events
65 (SSEs), enabling the investigation of SSE-related deformation characteristics near the trench axis
66 (e.g., Ito et al., 2013; Davis et al., 2015; Wallace et al., 2016).

67 SSEs are common to many subduction zones (e.g., Hirose et al., 1999; Heki & Kataoka,
68 2008; Wallace & Beavan, 2010; Nishimura et al., 2013; Ozawa, 2014). It is difficult to
69 characterize SSEs beneath the seafloor using land-based global navigation satellite system
70 (GNSS) networks, due to the lack of ability of onshore networks to resolve deformation
71 occurring on offshore faults. The advantage of OBPs is that the seafloor crustal deformation
72 associated with transient deformation, such as SSEs, can be continuously recorded with a

73 resolution of 1-3 centimeters (e.g., Ito et al., 2011; Davis et al., 2015; Suzuki et al., 2016;
74 Wallace et al., 2016; Fredrickson et al., 2019).

75 The greatest challenge associated with using OBPs for seafloor geodetic investigations to
76 detect cm-level vertical crustal deformation is the presence of oceanographic noise in seafloor
77 pressure data, which can be on the order of 1–2 meters for the tidal components, and tens of
78 centimeters for non-tidal components. To remove the oceanographic noise, two approaches are
79 commonly used: (1) oceanographic modeling to estimate and remove the non-tidal component
80 (Hino et al., 2014; Sato et al., 2017; Muramoto et al., 2019), and (2) a reference-station method
81 using pressure records from a reference station outside of the deforming zone to remove the
82 oceanographic noise under the assumption that the non-tidal components are common-mode over
83 a large region (Ito et al., 2013; Davis et al., 2015; Wallace et al., 2016; Frederickson et al., 2019).

84 The oceanographic modeling approach to reducing oceanographic noise in OBP data is
85 undertaken by subtracting the seafloor pressure predicted by the ocean model from the observed
86 pressure (e.g., Hino et al., 2014; Sato et al., 2017; Muramoto et al., 2019). Various modeling
87 approaches have been developed to calculate nontidal oceanographic variations, including a
88 global baroclinic ocean model using assimilated wind vector and heat flux (e.g., ECCO2), and
89 global barotropic ocean models driven by assimilated wind vectors and the sea surface pressures
90 (IN12) published by the 55-year Japanese Reanalysis Project (Kobayashi et al., 2015; Harada et
91 al., 2016). By applying the barotropic model, Hino et al. (2014) suppressed oceanographic noise
92 and detected crustal deformation (less than 5cm) associated with afterslip of the largest
93 foreshock following the 2011 Mw 9.0 Tohoku-Oki earthquake. At the Hikurangi subduction
94 zone, the variance reduction using the oceanographic models (~60%) was significantly less than
95 that obtained using reference sites for noise removal (~80-90%) (Muramoto et al., 2019),
96 suggesting that when suitable reference sites are available, the reference site approach is
97 generally more robust.

98 In the reference-station method, subtraction of the pressure data from the reference site
99 OBPs is commonly used assuming that the effects of oceanographic variability are largely
100 common-mode across the network footprint (e.g., Ito et al., 2013; Wallace et al., 2016). Adjacent
101 to the hypocenter of the 2011 Mw 9.0 Tohoku-Oki earthquake, crustal deformation of a few
102 centimeters due to slow slip was detected as relative vertical displacement, which was inferred
103 from pressure differences among several OBP pairs before the 2011 Tohoku-Oki earthquake (Ito
104 et al., 2013). At the northern Hikurangi subduction zone offshore the North Island of New
105 Zealand, Wallace et al. (2016) observed 1–5 cm of vertical crustal deformation during a
106 September/October 2014 SSE using OBP data (which was also observed by onshore GNSS
107 stations), and concluded that the slip may have reached the vicinity of the trench axis.
108 Fredrickson et al. (2019) recently demonstrated coherence in bottom pressure changes observed
109 between sites in similar water depths offshore Cascadia, leading them to propose a new method
110 of placing reference sites at common isobaths to achieve large reductions in oceanographic noise
111 in OBP time series. Here, we further evaluate the efficiency of considering differences between
112 bottom pressure pairs at a range of water depths using the OBP data acquired during a 2014–
113 2015 experiment offshore New Zealand.

114 2. Seafloor pressure data

115 We use data from OBPs deployed from mid-2014 to mid-2015 (Fig. 1) along the east
 116 coast of the North Island of New Zealand. These data originate from the Hikurangi Ocean
 117 Bottom Investigation of Tremor and Slow Slip (HOBITSS) experiment, which deployed 24
 118 autonomous OBPs and 15 ocean-bottom seismometers (OBS) aimed at investigating offshore
 119 SSEs and their relationship to tectonic tremor and earthquakes along the Hikurangi trough (e.g.,
 120 Wallace et al., 2016; Todd et al., 2018; Warren-Smith et al., 2019; Yarce et al., 2019; Yohler et
 121 al., 2019; Zal et al., 2020). The instruments in these dense arrays were deployed directly above
 122 the source region of shallow (< 10 km depth) slow slip events at the north Hikurangi margin
 123 (Wallace et al., 2016).

124 In general, pressure changes recorded by an OBP are described as a pressure P_{ref}
 125 corresponding to the water depth and a pressure deviation $\Delta P_B(t)$ that fluctuates around the
 126 pressure P_{ref} (Eq. (1)). A linear relationship between various components, including the crustal
 127 deformation component $\Delta P_C(t)$ (e.g., IN12), represents the seafloor pressure fluctuation $\Delta P_B(t)$
 128 (Eq. (2)), as follows:

$$P_B(t) = P_{ref} + \Delta P_B(t) \quad (1)$$

$$\Delta P_B(t) = \Delta P_C(t) + \Delta P_T(t) + \Delta P_O(t) + \Delta P_D(t) + \varepsilon(t) \quad (2)$$

129 where, $\Delta P_C(t)$ is the pressure change due to the vertical seafloor deformation, $\Delta P_T(t)$ is the
 130 pressure change due to the ocean tide and the Earth tides (mainly diurnal and semi-diurnal tides;
 131 ~ 100 hPa (Ray, 2013)), $\Delta P_O(t)$ is the pressure change due to nontidal oceanic variations such as
 132 ocean currents, eddies, and sea surface pressure changes (Ponte & Ray, 2002; ECCO2; IN12;
 133 Cummings & Smedstad, 2013), $\Delta P_D(t)$ is the pressure changes due to instrument drift (e.g.
 134 Kajikawa & Kobata, 2019), and $\varepsilon(t)$ is the unmodeled noise.

135 3. Coherent signals on bottom pressure between sites

136 We adopted two statistical quantities to evaluate the similarity between all pairs of OBP
 137 data in the HOBITSS experiment: (i) standard deviation (SD, Eq. (3)) of the residual pressure
 138 between a pair of sites and (ii) correlation coefficient (CC, Eq. (4)) between a pair of sites. After
 139 removing the tidal components and instrument drift from the observed data, we calculated both
 140 the SD and CC. Using the SD, CC, the depth and distance dependence of the pressure signals
 141 were evaluated within the HOBITSS OBP array (Table S1). The tides were removed by applying
 142 a low pass filter (cut off period: 2 days). Instrumental drift was estimated and removed by fitting
 143 an exponential and a linear term (see Fig. S1 for details) (Polster et al., 2009). The SD and CC
 144 equations are expressed as follows:

$$SD = \sqrt{\frac{1}{N} \sum_1^N (P_t^{ij} - A^{ij})^2} \quad (3)$$

$$CC = \frac{\sum_1^N (P_t^i - A^i)(P_t^j - A^j)}{\sqrt{\sum_1^N (P_t^i - A^i)^2} \sqrt{\sum_1^N (P_t^j - A^j)^2}} \quad (4)$$

145 where P_t^i and P_t^j denote the pressure anomaly at the time t at stations i and j , respectively. A^i and
 146 A^j denote the average of the time series of P_t^i and P_t^j , respectively. $P_t^{i,j}$ is the result of P_t^i minus
 147 P_t^j . A^{ij} is the average of the time series of the residual pressure ($P_t^{i,j}$), and N is the number of
 148 data in the time series.

149 **4. Relative water depth dependence on bottom pressure along an isobath**

150 We analyzed two time windows (185–265 days and 285–350 days from Jan. 1 2014),
 151 which did not include the two SSE periods in September/October 2014 (Wallace et al., 2016) and
 152 late December 2014 that were observed on nearby continuous GNSS data (Fig. S2). The OBP
 153 records after the second SSE were not analyzed due to a lack of data at some sites which stopped
 154 recording later in the experiment. We show example time series from pairs of OBP sites from
 155 days 185–265 at similar distances apart (~30 km) for 3 cases: (i) a large depth difference (1674
 156 m), (ii) an intermediate depth difference (579 m), and (iii) from sites at similar depth (depth
 157 difference: 114 m) (Fig. 2).

158 Non-tidal components observed on the OBPs in the HOBITSS network show strong
 159 similarities between site pairs at similar water depths (e.g., within 500–1000 m of each other).
 160 The similarity decreases with increasing relative depths between the sites (185–265 days in Figs.
 161 3a–3e, 285–350 days in Fig. S2a). In contrast, there appears to be very little dependence of the
 162 SD on the horizontal distance between site pairs (maximum distance between sites ~75 km), as
 163 no significant increase in the SD as a function of the inter-site distance was observed (185–265
 164 days in Fig. 3f–3j, 285–350 days in Fig. S3). An R value of 0.57 was calculated for the
 165 correlation between the SD of pair-wise residual pressure versus the relative depth difference
 166 (Fig. 3a), compared with a value of 0.17 for the correlation of the residual pressure versus the
 167 inter-site distance (Fig. 3f). The correlations depended on the depths of the sites. In addition, the
 168 R values were calculated for the scatter plot of the SD against the depth of the deeper site in each
 169 pair, with results of 0.45, 0.86, 0.86, and 0.81 for depth ranges of less than 1300 m, 1300–2000
 170 m, 2000–2500 m, and more than 2500 m, respectively. This suggests that the bottom pressure
 171 data from site pairs deeper than 1300 m are much more strongly correlated, and that larger depth
 172 separations between such site pairs may be suitable for enhanced oceanographic noise removal.
 173 Similarly, the R value of -0.52 is calculated from the scatter distribution of CC as a function of
 174 relative water depth difference (185–265 days in Figs. S4a–S4e, 285–350 days in Figs. S5a). In
 175 contrast, an R value of -0.13 is calculated as a function of inter-site distance (185–265 days in
 176 Figs. S4f–S4j, 285–350 days in Fig. S5b). The CC shows a strong dependence on depth
 177 difference (185–265 days in Fig. S4, 285–350 days in Fig. S5), further indicating that the
 178 similarity in nontidal components observed in ocean bottom pressure depends on relative water
 179 depth, but not on relative distance.

180 The pair-wise SDs calculated from the HOBITSS data were grouped according to
 181 whether the values fall under a certain threshold (less than 0.5, 1.0, and 1.5 hPa), and these were
 182 found to vary widely depending on the depth of the deeper site of the site pairs (Figs. 3, 4). The
 183 SDs from the shallower pairs where the deeper site is located at less than 2500 m rapidly
 184 increase with increasing depth difference, suggesting that for sites in < 2500 m water depth,
 185 reference sites within 500-1000 m water depth of other sites are needed to reduce the
 186 oceanographic noise levels to below 1–1.5 hPa, and a depth difference of < 250 m is required to
 187 reduce this to < 0.5 hPa (e.g., Figs. 3b–3d, 4a). In contrast, the SDs from the pairs with the
 188 deeper depths (> 2500 m) increase more gradually—remaining < 1 hPa even with the depth

189 differences of 2200 m (Figs. 3e, 4a). This suggests that for deeper sites (e.g., located at depths >
190 2500 m), reference sites from a broader range of depths can be utilized.

191 Viewing the results in terms of a normalized water depth range, calculated by dividing
192 the depth range by the depth of deepest site (of the pair) (Fig. 4), is also a useful guide for
193 reference site selection. To achieve SDs < 1hPa, for instance, the depth range of the pair must be
194 within a normalized depth of approximately 0.5, or less than half the depth of the deepest site
195 (Fig. 4b). However, for the deep site LOBS4 (3441 m depth), SDs less than 1.0 and 1.5 hPa are
196 calculated for reference sites that are 2194 m and 2451 m shallower than LOBS4 (Fig. 4a). For
197 SBPR2 (2116 m depth), SDs less than 0.5, 1.0 and 1.5 hPa are calculated using sites that are 243
198 m, 672 m and 1127 m shallower than SBPR2, respectively (Fig. 4a). For LOBS9 (1457 m depth),
199 SDs less than 0.5, 1.0 and 1.5 hPa are calculated using sites at 211 m, 469 m and 806 m
200 shallower than LOBS9, respectively. This suggests that site pairs with depth differences < 250 m
201 are required if the very low noise levels (e.g., < 0.5 hPa, or < 5 mm) are desired (Fig. 4a).
202 Overall, in the region of HOBITSS experiment, normalized depth ranges of 0.2, 0.5 and 0.7 are
203 required when targeting SDs less than 0.5, 1.0 and 1.5, respectively (Fig. 4b). These
204 characteristics of the HOBITSS OBP data provide a useful indicator for network design
205 strategies which aim for the detection of cm-level crustal deformation from SSEs, and to help
206 guide the design of future OBP networks in New Zealand, and at similar settings.

207 We also evaluate the water depth dependence of non-tidal components predicted by
208 oceanographic models at the OBP sites using both the baroclinic (ECCO2) and barotropic (IN12)
209 models. The baroclinic ECCO2 model shows similar relative water depth dependence for the
210 predicted differences in ocean bottom pressure records to those in the observed data (Figs. 3a and
211 S6a). In contrast, the dependence on the relative water depth is not significant in the barotropic
212 model (Figs. 3a and S6c). Neither model produces a relative distance dependence, similar to the
213 observed pressure data (Figs. S6b and S6d). The higher R value in the ECCO2 (0.71) relative to
214 IN12 (0.36) indicates that much of the non-tidal component in the observed pressure may
215 originate from baroclinic effects. This result suggests that the baroclinic model reproduces the
216 dependence on relative water depth of actual nontidal components better than the barotropic
217 models. Furthermore, it hints that in terms of the depth dependence of the nontidal variations, the
218 baroclinic models are required if oceanographic models are to be used to correct nontidal effects
219 in OBP data.

220 Taking the difference between pairs of data at similar water depths can reduce
221 oceanographic noise in the pressure data to less than 1 hPa, which corresponds to 1 cm in terms
222 of the relative vertical deformation (Figs. 3, 4). Previous estimates of seafloor vertical
223 deformation use reference sites seaward of the trench (TXBPR1 and LOBS4; ~3500 m deep) and
224 shows a minimum standard deviation of 0.52 hPa at the deepest site SBPR1 (2453 m deep;
225 Wallace et al., 2016). Previously estimated standard deviations were 1.53 and 1.41 hPa at the
226 sites shallower than 1000 m (TXBPR2 and LOBS8, respectively) when using reference sites on
227 the incoming plate (Muramoto et al., 2019). Using an ocean model (WCOFS - Kurapov et al.,
228 2017) to simulate seafloor pressure records, residuals in Cascadia were estimated to be less than
229 1 hPa RMS (e.g., < 1 cm) when taking the difference between model sites at similar depths
230 whose range vary with depth (e.g., within 1000m for sites on the abyssal plain) even for sites
231 spaced far apart (< 326 km) (Fredrickson et al., 2019). Those results are comparable to what we
232 observe at the Hikurangi subduction zone. In an OBP network with a higher density of sites, such
233 as the HOBITSS array (which has a maximum site spacing of ~75 km), we clearly demonstrate

234 that the observed nontidal components have a similarly strong relative water depth dependence,
235 even for the case of a much smaller site spacing such as ours. This reinforces the idea proposed
236 by Frederickson et al. (2019) that the most effective way of utilizing reference sites is to have
237 these sites in similar water depths as the other sites in the areas of interest which are above the
238 zones of deformation, also holds for networks that are relatively dense. For example, for a
239 network, such as HOBITSS, which targets SSEs in a particular area, reference sites along-strike
240 of the SSE region, but at similar water depths to the sites above the SSE area, are the most
241 effective at the removal of oceanographic noise.

242 **5. Conclusions**

243 Using data from a 2014/2015 OBP experiment offshore New Zealand, we showed that
244 the non-tidal components of seafloor pressure are similar along isobaths in the Hikurangi
245 subduction zone. When using the full range of reference site pairs, we found that the standard
246 deviation values for the residual pressure between the site pairs depends strongly on the
247 difference in the depths of the site pairs. The dependence of standard deviation on the water
248 depth difference between the pairs is strong ($R=0.57$), confirming the previous suggestion of
249 Frederickson et al. (2019) that strong similarities in nontidal oceanographic signals exist between
250 sites at comparable water depths, and that this characteristic can be used to optimize OBP
251 network design for seafloor geodetic investigations. We also found that the similarities of bottom
252 pressure signals have little dependence on the distances between site pairs. To reduce noise
253 levels to below 1 hPa in 2500 m of water depth or less, the water depth difference between site
254 pairs must be < 1000 m. At water depths greater than 2500 m, the oceanographic similarities are
255 greater over larger depth ranges, suggesting that in these cases, reference sites within 2200 m
256 water depth of each other may be suitable for oceanographic noise removal, if targeting < 1 hPa
257 residual noise levels. If targeting even lower noise levels, smaller depth differences between
258 reference sites and the rest of the network will be needed. The simulated non-tidal component of
259 the pressure residuals at the sites as calculated from a baroclinic oceanographic circulation model
260 also showed a strong dependence on depth, as compared with the dependence on the distance. In
261 contrast, barotropic models are unable to reproduce the depth-dependent similarities in non-tidal
262 oceanographic variations, suggesting that in terms of the depth dependence of the nontidal
263 variations, baroclinic models produce a more accurate representation of nontidal signals
264 observed on bottom pressure records. Similar to previous studies in Cascadia, our results
265 highlight the need to consider the placement of reference sites when designing OBP networks
266 with the intent of capturing cm-level transient deformation events, which can be achieved by
267 installing those reference sites at water depths similar to other sites in the rest of the network.

268

269 **Acknowledgments**

270 This research was supported by the Japan Society for the Promotion of Science KAKENHI
271 program [grant no. 26257206] for Y.I. and the Japan Science and the Technology Agency–Japan
272 International Cooperation Science and Technology Research Partnership for Sustainable
273 Development [grant no. JPMJSA1510], and an NZ MBIE Endeavour fund grant, and NSF
274 grants. We thank the captain and crew of the R/V Tangaroa and the R/V Revelle for deployment
275 and recovery of ocean bottom pressure recorders. The deployment was supported by the NSF
276 grants to Wallace and Webb (OCE- 1334654 and OCE-1333311). Support for ship time came

277 from NSF, GNS Science, and the New Zealand government-funded Oceans 2020 program. The
 278 authors declare that there are no conflicts of interest. The Generic Mapping Tools software v.
 279 5.3.1 (Wessel et al., 2013) was used to prepare the figures. Data are available from the server
 280 managed by the authors upon request as well as on the IRIS website (<https://www.iris.edu/hq/>).

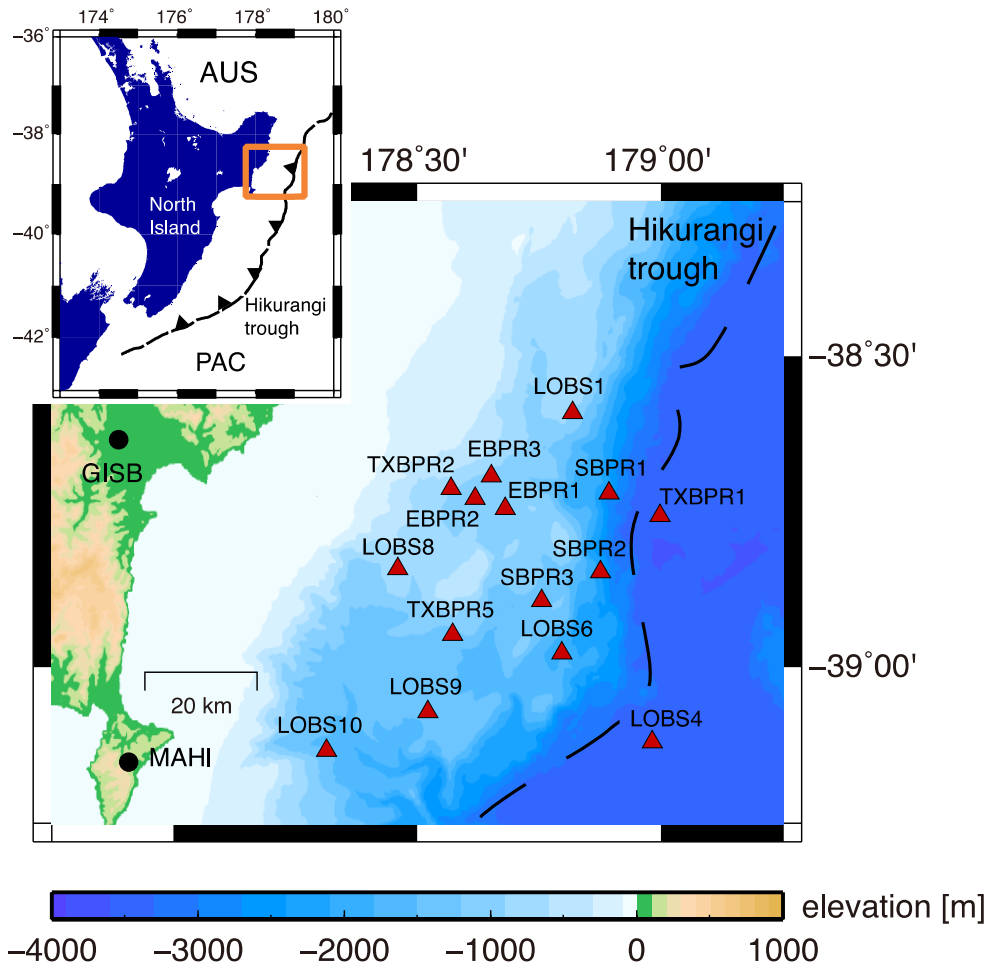
281 **References**

- 282 Cummings, J. A., & Smedstad, O. M. (2013). Variational Data Assimilation for the Global
 283 Ocean. *Data Assimilation for Atmospheric, Oceanic and Hydrologic Applications, II*, 303–
 284 343. <https://doi.org/10.1007/978-3-642-35088-7>
- 285 Davis, E. E., Villinger, H., & Sun, T. (2015). Slow and delayed deformation and uplift of the
 286 outermost subduction prism following ETS and seismogenic slip events beneath Nicoya
 287 Peninsula, Costa Rica. *Earth and Planetary Science Letters*, *410*, 117–127.
 288 <https://doi.org/10.1016/j.epsl.2014.11.015>
- 289 Fredrickson, E. K., Wilcock, W. S. D., Schmidt, D. A., MacCready, P., Roland, E., Kurapov, A.
 290 L., et al. (2019). Optimizing Sensor Configurations for the Detection of Slow-Slip
 291 Earthquakes in Seafloor Pressure Records, Using the Cascadia Subduction Zone as a Case
 292 Study. *Journal of Geophysical Research: Solid Earth*.
 293 <https://doi.org/10.1029/2019JB018053>
- 294 Harada, Y., Kamahori, H., Kobayashi, C., Endo, H., Kobayashi, S., Ota, Y., et al. (2016). The
 295 JRA-55 reanalysis: Representation of atmospheric circulation and climate variability.
 296 *Journal of the Meteorological Society of Japan*, *94*(3), 269–302.
 297 <https://doi.org/10.2151/jmsj.2016-015>
- 298 Heki, K., & Kataoka, T. (2008). On the biannually repeating slow-slip events at the Ryukyu
 299 Trench, southwestern Japan. *Journal of Geophysical Research: Solid Earth*, *113*(11), 1–12.
 300 <https://doi.org/10.1029/2008JB005739>
- 301 Hino, R., Inazu, D., Ohta, Y., Ito, Y., Suzuki, S., Iinuma, T., et al. (2014). Was the 2011 Tohoku-
 302 Oki earthquake preceded by aseismic preslip? Examination of seafloor vertical deformation
 303 data near the epicenter. *Marine Geophysical Research*, *35*(3), 181–190.
 304 <https://doi.org/10.1007/s11001-013-9208-2>
- 305 Hirose, H., Hirahara, K., Kimata, F., Fujii, N., & Miyazaki, S. (1999). A slow thrust slip event
 306 following the two 1996 Hyuganada earthquakes beneath the Bungo Channel, southwest
 307 Japan. *Geophysical Research Letters*, *26*(21), 3237–3240.
 308 <https://doi.org/10.1029/1999GL010999>
- 309 Inazu, D., Hino, R., & Fujimoto, H. (2012). A global barotropic ocean model driven by synoptic
 310 atmospheric disturbances for detecting seafloor vertical displacements from in situ ocean
 311 bottom pressure measurements. *Marine Geophysical Research*, *33*(2), 127–148.
 312 <https://doi.org/10.1007/s11001-012-9151-7>
- 313 Ito, Y., Tsuji, T., Osada, Y., Kido, M., Inazu, D., Hayashi, Y., et al. (2011). Frontal wedge
 314 deformation near the source region of the 2011 Tohoku-Oki earthquake. *Geophysical*
 315 *Research Letters*, *38*(15), 1–5. <https://doi.org/10.1029/2011GL048355>
- 316 Ito, Y., Hino, R., Kido, M., Fujimoto, H., Osada, Y., Inazu, D., & Ashi, J. (2013). Episodic slow
 317 slip events in the Japan subduction zone before the 2011 Tohoku-Oki earthquake.
 318 *Tectonophysics*, (600), 14–26. Retrieved from <http://dx.doi.org/10.1016/j.tecto.2012.08.022>
- 319 Kajikawa, H., & Kobata, T. (2019). Evaluation and correction for long-term drift of hydraulic
 320 pressure gauges monitoring stable and constant pressures. *Measurement: Journal of the*

- 321 *International Measurement Confederation*, 134, 33–39.
322 <https://doi.org/10.1016/j.measurement.2018.10.051>
- 323 Kobayashi, S., Ota, Y., Harada, Y., Ebita, A., Moriya, M., Onoda, H., et al. (2015). The JRA-55
324 reanalysis: General specifications and basic characteristics. *Journal of the Meteorological*
325 *Society of Japan*, 93(1), 5–48. <https://doi.org/10.2151/jmsj.2015-001>
- 326 Kurapov, A. L., Erofeeva, S. Y., & Myers, E. (2017). Coastal sea level variability in the US West
327 Coast Ocean Forecast System (WCOFS). *Ocean Dynamics*, 67(1), 23–36.
328 <https://doi.org/10.1007/s10236-016-1013-4>
- 329 Menemenlis, D., Campin, J.-M., Heimbach, P., Hill, C. N., Lee, T., Nguyen, A. T., et al. (2008).
330 ECCO2: High resolution global ocean and sea ice data synthesis. *Mercator Ocean*
331 *Quarterly Newsletter*, 31(October), 13–21. Retrieved from [http://www.mercator-](http://www.mercator-ocean.fr/content/download/691/5904/version/1/file/lettre_31_en.pdf#page=13)
332 [ocean.fr/content/download/691/5904/version/1/file/lettre_31_en.pdf#page=13](http://www.mercator-ocean.fr/content/download/691/5904/version/1/file/lettre_31_en.pdf#page=13)
- 333 Muramoto, T., Ito, Y., Inazu, D., Wallace, L. M., Hino, R., Suzuki, S., et al. (2019). Seafloor
334 Crustal Deformation on Ocean Bottom Pressure Records With Nontidal Variability
335 Corrections: Application to Hikurangi Margin, New Zealand. *Geophysical Research*
336 *Letters*, 46(1), 303–310. <https://doi.org/10.1029/2018GL080830>
- 337 Nishimura, T., Matsuzawa, T., & Obara, K. (2013). Detection of short-term slow slip events
338 along the Nankai Trough, southwest Japan, using GNSS data. *Journal of Geophysical*
339 *Research: Solid Earth*, 118(6), 3112–3125. <https://doi.org/10.1002/jgrb.50222>
- 340 Ozawa, S. (2014). Shortening of recurrence interval of Boso slow slip events in Japan.
341 *Geophysical Research Letters*, 41(8), 2762–2768. <https://doi.org/10.1002/2014GL060072>
- 342 Polster, A., Fabian, M., & Villinger, H. (2009). Effective resolution and drift of paroscientific
343 pressure sensors derived from long-term seafloor measurements. *Geochemistry,*
344 *Geophysics, Geosystems*, 10(8). <https://doi.org/10.1029/2009GC002532>
- 345 Ponte, R. M., & Ray, R. D. (2002). Atmospheric pressure corrections in geodesy and
346 oceanography: A strategy for handling air tides. *Geophysical Research Letters*, 29(24), 6-1-
347 6-4. <https://doi.org/10.1029/2002gl016340>
- 348 Ray, R. D. (2013). Precise comparisons of bottom-pressure and altimetric ocean tides. *Journal of*
349 *Geophysical Research: Oceans*, 118(9), 4570–4584. <https://doi.org/10.1002/jgrc.20336>
- 350 Sato, T., Hasegawa, S., Kono, A., Shiobara, H., Yagi, T., Yamada, T., et al. (2017). Detection of
351 vertical motion during a slow-slip event off the Boso Peninsula, Japan, by ocean bottom
352 pressure gauges. *Geophysical Research Letters*, 44(6), 2710–2715.
353 <https://doi.org/10.1002/2017GL072838>
- 354 Suzuki, K., Nakano, M., Takahashi, N., Hori, T., Kamiya, S., Araki, E., et al. (2016).
355 Synchronous changes in the seismicity rate and ocean-bottom hydrostatic pressures along
356 the Nankai trough: A possible slow slip event detected by the Dense Oceanfloor Network
357 system for Earthquakes and Tsunamis (DONET). *Tectonophysics*, 680, 90–98.
358 <https://doi.org/10.1016/j.tecto.2016.05.012>
- 359 Todd, E. K., Schwartz, S. Y., Mochizuki, K., Wallace, L. M., Sheehan, A. F., Webb, S. C., et al.
360 (2018). Earthquakes and Tremor Linked to Seamount Subduction During Shallow Slow Slip
361 at the Hikurangi Margin, New Zealand. *Journal of Geophysical Research: Solid Earth*,
362 123(8), 6769–6783. <https://doi.org/10.1029/2018JB016136>
- 363 Wallace, L., Webb, S., Ito, Y., Mochizuki, K., Hino, R., Henrys, S., et al. (2016). Slow slip near
364 the trench at the Hikurangi subduction zone, New Zealand. *Science*, 352(6286), 701–704.
365 <https://doi.org/10.1126/science.aaf2349>

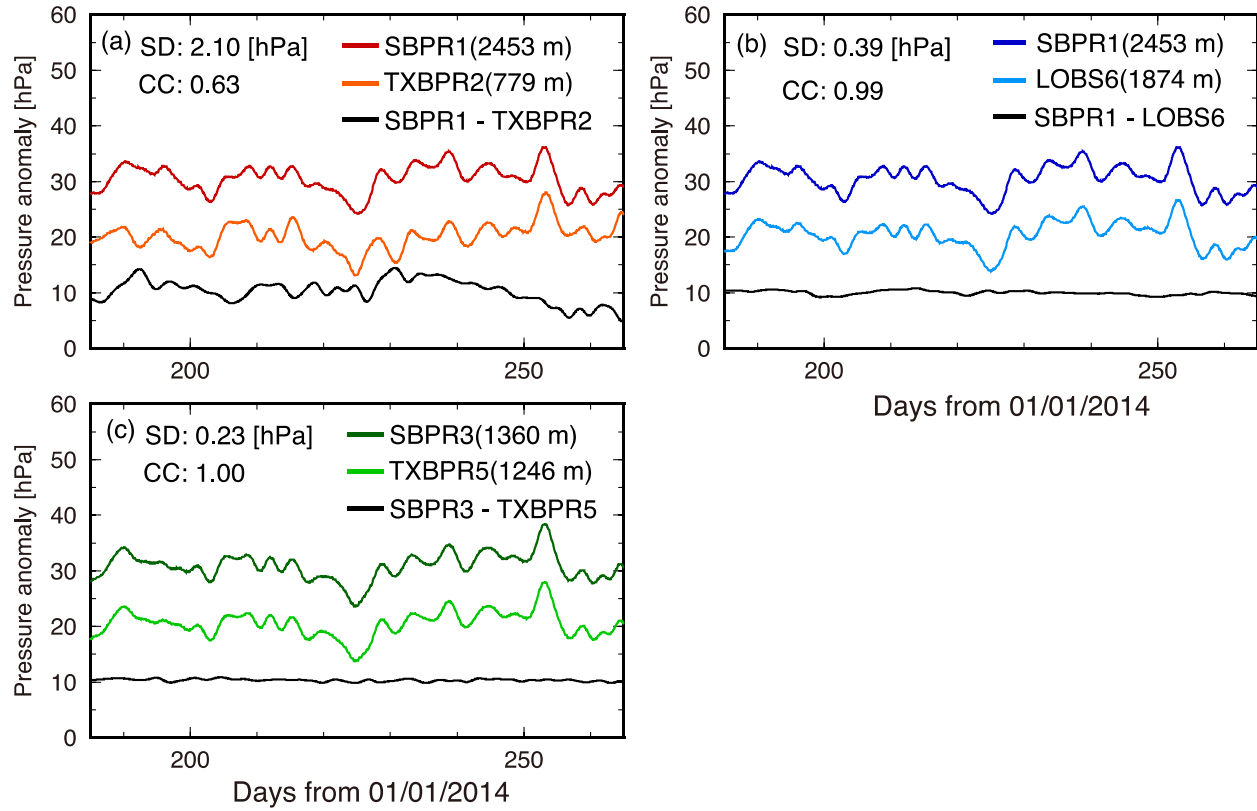
- 366 Wallace, L. M., & Beavan, J. (2010). Diverse slow slip behavior at the Hikurangi subduction
367 margin, New Zealand. *Journal of Geophysical Research: Solid Earth*, *115*(12), 1–20.
368 <https://doi.org/10.1029/2010JB007717>
- 369 Warren-Smith, E., Fry, B., Wallace, L., Chon, E., Henrys, S., Sheehan, A., et al. (2019). Episodic
370 stress and fluid pressure cycling in subducting oceanic crust during slow slip. *Nature*
371 *Geoscience*, *12*(6), 475–481. <https://doi.org/10.1038/s41561-019-0367-x>
- 372 Wessel, P., Smith, W. H. F., Scharroo, R., Luis, J., & Wobbe, F. (2013). Generic mapping tools:
373 Improved version released. *Eos*, *94*(45), 409–410. <https://doi.org/10.1002/2013EO450001>
- 374 Yarce, J., Sheehan, A. F., Nakai, J. S., Schwartz, S. Y., Mochizuki, K., Savage, M. K., et al.
375 (2019). Seismicity at the Northern Hikurangi Margin, New Zealand, and Investigation of
376 the Potential Spatial and Temporal Relationships With a Shallow Slow Slip Event. *Journal*
377 *of Geophysical Research: Solid Earth*, *124*(5), 4751–4766.
378 <https://doi.org/10.1029/2018JB017211>
- 379 Yohler, R., Bartlow, N., Wallace, L. M., & Williams, C. (2019). Time-Dependent Behavior of a
380 Near-Trench Slow-Slip Event at the Hikurangi Subduction Zone. *Geochemistry,*
381 *Geophysics, Geosystems*, *20*(8), 4292–4304. <https://doi.org/10.1029/2019GC008229>
- 382 Zal, H. J., Jacobs, K., Savage, M. K., Yarce, J., Mroczek, S., Graham, K., et al. (2020). Temporal
383 and spatial variations in seismic anisotropy and VP/VS ratios in a region of slow slip. *Earth*
384 *and Planetary Science Letters*, *532*, 115970. <https://doi.org/10.1016/j.epsl.2019.115970>
385
386

387



388

389 **Figure 1.** Map of the study area and the network map of the OBP gauges. Triangles and circles
 390 indicate stations for OBP and land GNSS sites, respectively. AUS and PAC indicate the
 391 Australian and Pacific plates, respectively.

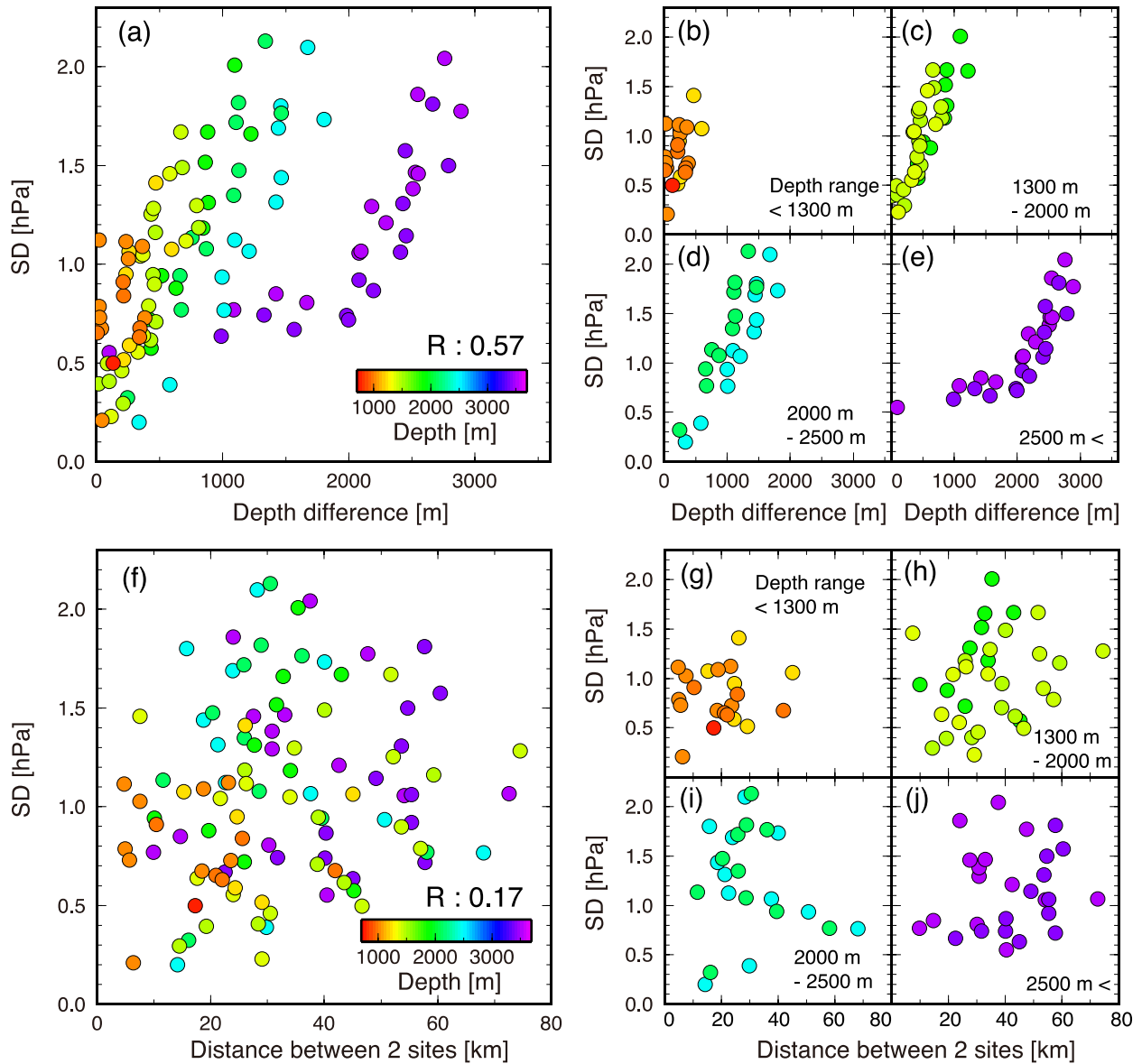


392

393 **Figure 2.** An example of the OBP time series. (a) Site pairs with a large difference in depth
 394 (depth difference: 1674 m) and a 28.2 km distance between sites. (b) Site pairs with similar
 395 depths (depth difference: 579 m) with a 29.1 km distance between sites. (c) Site pairs with
 396 similar depths (depth difference: 114 m) with a 29.1 km distance between sites.

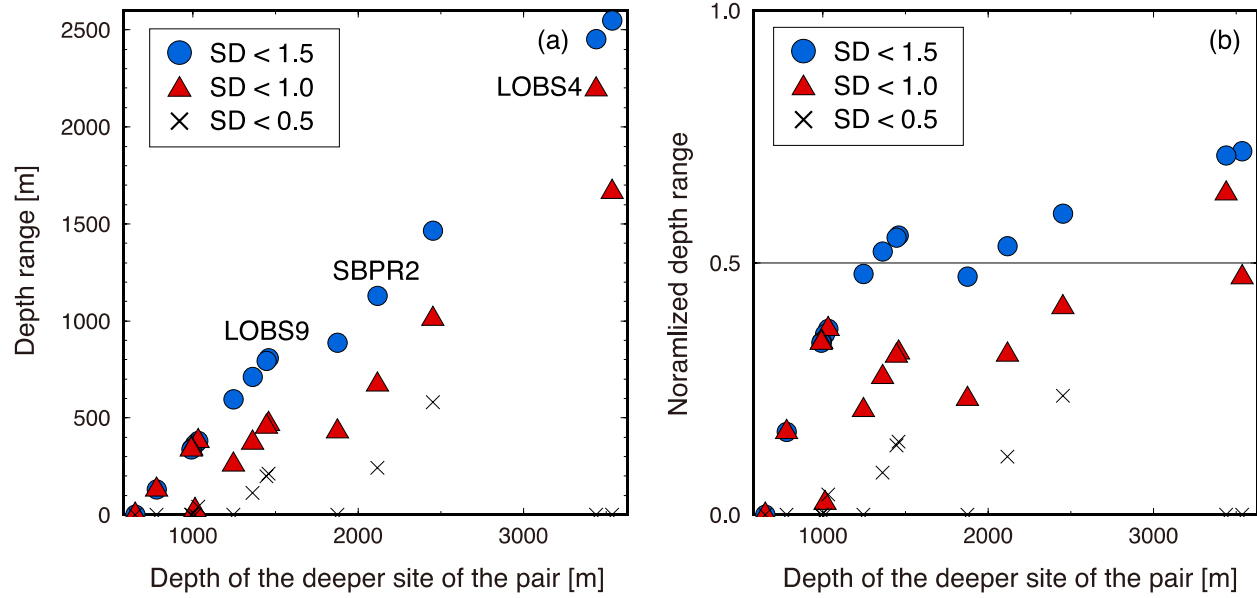
397

398



399

400 **Figure 3.** The relationship between the standard deviation (SD) of the residual observed pressure
 401 in the period (185–265 days) and the absolute depth difference (a–e) and the distance (f–j)
 402 between two sites. Colored circles indicate the depth of the deeper site of each pair of sites (a–j).
 403 The R value indicates the correlation coefficient of the distribution between SD and depth
 404 difference (a) or the distances between the 2 sites (f). (b–e) and (g–j) are separated into four sets
 405 of site depths, using the data from (a) and (f).
 406



407

408 **Figure 4.** (a) Comparison of the SD (blue circle: < 1.5 hPa, red triangle: < 1.0 hPa, and black
 409 cross: < 0.5hPa) thresholds for the depth ranges relative to the depth of the deepest site of the
 410 pairs. (b) Comparison of the SDs for normalized depth ranges relative to the depth of the deepest
 411 site of the pairs. Normalized depth is calculated by dividing the depth range by each depth of the
 412 deepest site of the pairs.

413

414